JACS
JOURNAL OF THE AMERICAN CHEMICAL SOCIETY
pubs.acs.org/JACS
Article

Fluorous Soluble Cyanine Dyes for Visualizing Perfluorocarbons in Living Systems

Irene Lim, Antoine Vian, Heidi L. van de Wouw, Rachael A. Day, Carlos Gomez, Yucen Liu, Arnold L. Rheingold, Otger Campàs,* and Ellen M. Sletten*

Cite This: https://dx.doi.org/10.1021/jacs.0c07761
Read Online

ABSTRACT: The bioorthogonal nature of perfluorocarbons provides a unique platform for introducing dynamic nano- and microdroplets into cells and organisms. To monitor the localization and deformation of the droplets, fluorous soluble fluorophores that are compatible with standard fluorescent protein markers and applicable to cells, tissues, and small organisms are necessary. Here, we introduce fluorous cyanine dyes that represent the most red-shifted fluorous soluble fluorophores to date. We study the effect of covalently appended fluorous tags on the cyanine scaffold and evaluate the changes in photophysical properties imparted by the fluorous phase. Ultimately, we showcase the utility of the fluorous soluble pentamethine cyanine dye for tracking the localization of perfluorocarbon nanoemulsions in macrophage cells and for measurements of mechanical forces in multicellular spheroids and zebrafish embryonic tissues. These studies demonstrate that the red-shifted cyanine dyes offer spectral flexibility in multiplexed imaging experiments and enhanced precision in force measurements.

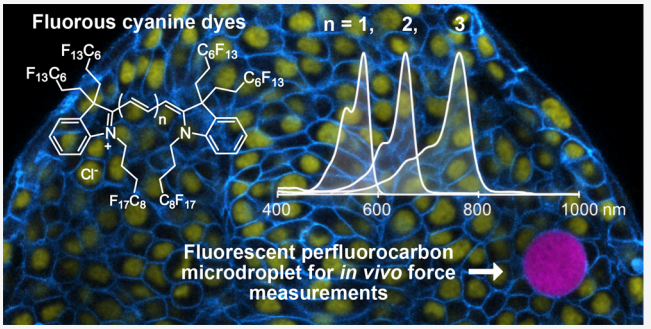

INTRODUCTION

Highly fluorinated compounds, referred to as fluorous,[1] phase separate from aqueous and organic solution, which renders them orthogonal to natural products and biomolecules[2,3] (Figure 1A). The noncovalent bioorthogonality[4,5] of the fluorous phase, coupled with the inertness of the C−F bond, have resulted in rising applications of perfluorocarbons in biology and medicine, including microarray assembly,[6] antibiofouling coatings,[7] oxygen delivery,[8] ultrasound and magnetic resonance imaging diagnostics,[9] and *in vivo* force measurements.[10] As the utility of fluorinated materials expands, the chemical tools available to analyze and track the fluorous phase must also evolve.

Fluorescence microscopy is a simple and ubiquitous analytical method, which allows for multiple species to be imaged simultaneously if the fluorophores have distinct photophysical properties.[11] To maximize signal, it is advantageous to employ fluorophores that are well-matched to excitation sources on standard microscopes. For biological applications, fluorophores that are complementary to standard fluorescent proteins commonly used to denote cellular structures are desirable. Imaging in animals and three-dimensional tissues provides further challenges where red-shifted fluorophores are needed to minimize background autofluorescence and light scattering.[12] Here, we develop red-shifted fluorous fluorophores that are well-matched to common laser lines for confocal microscopy and can be employed alongside ubiquitous cell markers, to facilitate advanced applications of the fluorous phase.

There have been a handful of fluorophores synthesized over the past decade that contain greater than 50 weight % fluorine (wt% F). Fluorinated variants, deemed "fluorofluorophores",[13] of multiple chromophore classes have been prepared, including polycyclic aromatic hydrocarbon,[14] coumarin,[15,16] porphyrin,[17] perylene bisimide,[18] rhodamine,[19] phthalocyanine,[20,21] and BODIPY[22] scaffolds (Figure 1B). Despite the high wt% F, many of these fluorophores are not soluble in perfluorocarbons, solvents that are composed of purely carbon and fluorine.[1−3] This is likely a result of the large polarizable π-systems present in chromophores, which do not interact favorably with the nonpolarizable fluorous phase.[2,23] Currently, there are no fluorophores with a $\lambda_{max,em}$ above 600 nm that are soluble in perfluorocarbons. Furthermore, only the anthracene, perylene bisimide, and rhodamine fluorofluorophores have had their photophysical properties characterized in fluorous solvent.[14,18,19]

Received: July 18, 2020
Published: August 18, 2020

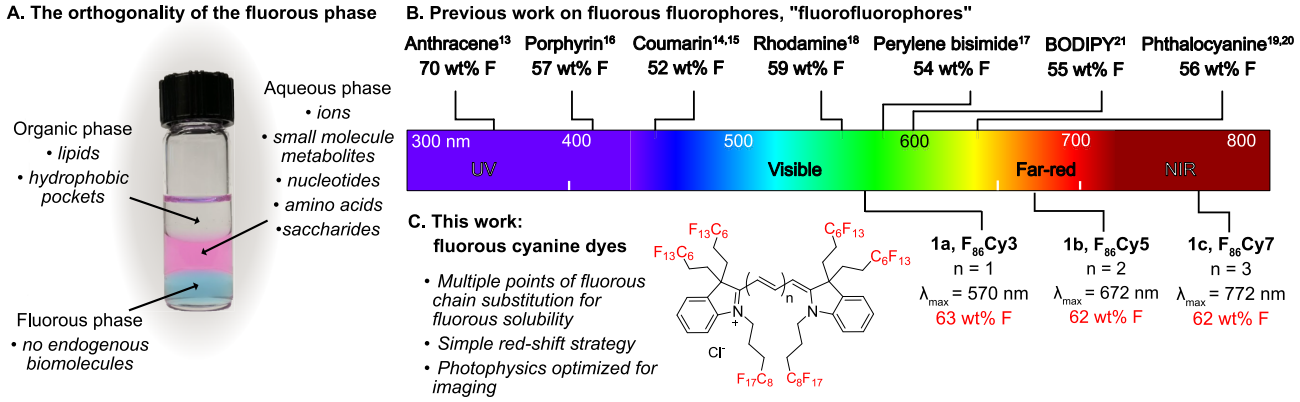

Figure 1. (A) Perfluorocarbons form an orthogonal phase relative to hydrophilic and lipophilic compounds. In the vial are hexane (organic phase, top, colorless), water containing Rose Bengal (aqueous phase, middle, pink), and perfluorohexane containing **1b** (fluorous phase, bottom, blue). Typical biomolecules that associate with each phase are indicated in italics. (B) Fluorofluorophores in the literature with greater than 50 wt% F placed on an electromagnetic spectrum corresponding to their λ_{max} absorbance. See Figure S1 for full structures of the fluorophores. (C) Fluorous cyanine dyes reported in this Article, deemed F_{86}Cy dyes (**1a**–**1c**).

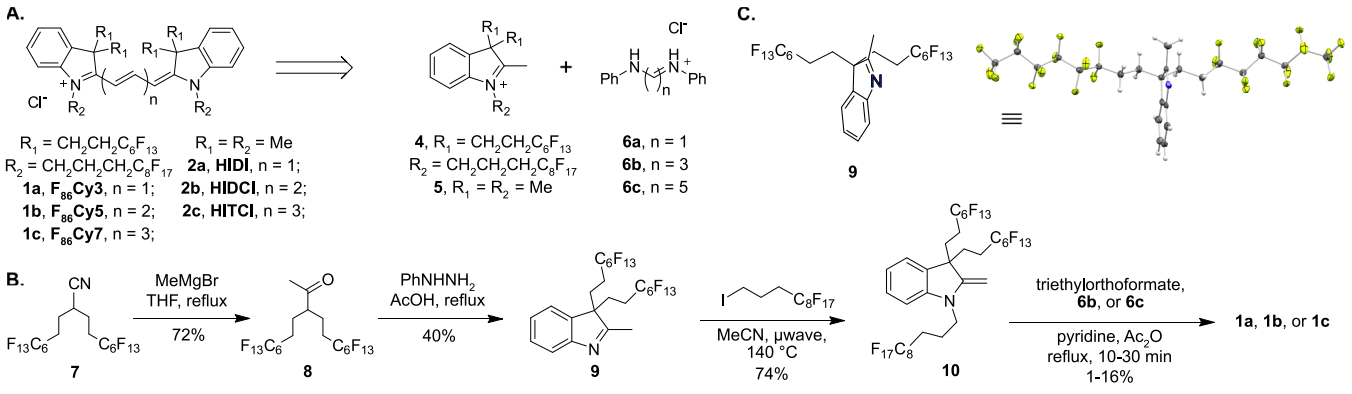

Figure 2. Synthesis of cyanine dyes. (A) Retrosynthetic analysis of cyanine dyes, formed by condensation of a polymethine linker with an indolinium heterocycle. Dyes made with all methyl substituents on indolinium are abbreviated HIDI (**2a**), HIDCI (**2b**), and HITCI (**2c**). Dyes with all fluorous substituents are named F_{86}Cy3 (**1a**), F_{86}Cy5 (**1b**), and F_{86}Cy7 (**1c**). (B) Synthesis of F_{86}Cy dyes **1a**–**1c**. (C) Crystal structure of indolenine **9**, which shows the position of the fluorous substituents relative to the plane of the indolenine. Ellipsoids are set at 50% probability. A perspective structure is provided to the left.

In this Article, we report a series of cyanine fluorofluorophores with greater than 60 wt% F (Figure 1C, **1a**–**1c**). The reported cyanine dyes represent the most red-shifted fluorofluorophores to date with $\lambda_{max,abs}$ = 571 nm (visible region), 672 nm (far-red region), and 781 nm (NIR, near-infrared region). We analyze the photophysical consequences of the addition of fluorous tags to the cyanine chromophore by comparing **1a**–**1c** to commercial nonfluorinated analogues (**2a**–**2c**, Figure 2A). We also characterize the solubility and photophysical properties of the cyanine fluorofluorophores in perfluorocarbon solvents, with comparisons to fluorous rhodamine **3** (Figure 3A). Rhodamine **3** is currently employed for visualizing the fluorous phase in living systems.[24,25] Finally, we showcase the utility of cyanine **1b** for multiplexed microscopy of perfluorocarbon nanoemulsions in cells and for force measurements in 3D spheroids and zebrafish embryonic tissues using perfluorocarbon microdroplets.

RESULTS AND DISCUSSION

Design and Synthesis of Cyanine Fluorofluorophores. The most prevalent cyanine dyes contain indoline heterocycles and are prepared through the condensation of indolinium salts and polymethine electrophiles (Figure 2A). One heterocycle allows access to a family of cyanine dyes by modulating the length of the polymethine chain. The ability to reliably bathochromically shift the absorbance and emission by the addition of a small vinylene unit[26] makes cyanine dyes an opportune scaffold for the creation of red-shifted fluorofluorophores, as the wt% F is minimally altered to implement a 100 nm shift. As such, we focused on the creation of a fluorous indolinium heterocycle (**4**), which could be transformed into multiple fluorophores that span the visible and NIR regions of the electromagnetic spectrum.

To maximize fluorous solubility, multiple fluorous tags are included on each heterocycle. The tags surround the chromophore when placed in fluorous solvent. This approach was based on previous work that has demonstrated polarizable aromatic π-systems often require multiple sites of incorporation of fluorous tags to induce perfluorocarbon solubility.[23,27] As classic cyanine dyes require disubstitution of the 3-position of the indolinium and alkylation of the nitrogen to create the chromophore scaffold, these positions were the most logical points of introduction of fluorous tags. Consequently, indolinium **4**, containing three fluorous tags, became our key intermediate (Figure 2A).

Indolenines, the synthetic precursor to indolinium salts, are obtained through a Fischer indole cyclization of phenyl hydrazine and a 3,3-disubstituted methyl ketone, which in

https://dx.doi.org/10.1021/jacs.0c07761
J. Am. Chem. Soc. XXXX, XXX, XXX−XXX

A.

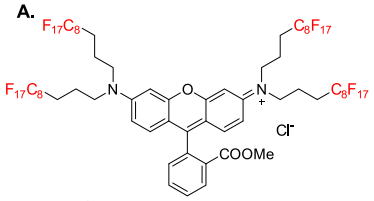

3, Fluorous Rhodamine

B.

	$\log_F\left(\frac{\text{PFMC}}{\text{Toluene}}\right)$	Solubilities in acetone		Solubilities in PFMC	
		Abs (mM)	Relative	Abs (mM)	Relative
1a	1.82	0.91	10.7	0.12	11
1b	0.157	0.11	1.3	0.21	8
1c	2.35	0.09	1	0.04	3
3	1.42	0.15	1.7	0.01	1

C.

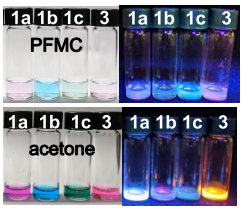

D.

Solvents	$\lambda_{max,abs}$ (nm)			$\lambda_{max,em}$ (nm)			ε (x 10^3 $M^{-1}cm^{-1}$)			ϕ_F		
	1a	**1b**	**1c**	**1a**	**1b**	**1c**	**1a**	**1b**	**1c**	**1a**	**1b**	**1c**
EtOH	570	656	758	588	682	790	38.3	228	180	0.115	0.291	0.16
acetone	571	655	762	591	677	792	105	182	199	0.109	0.573	0.20
DCM	a	672	773	a	691	800	a	81	254	a	0.59	0.22
PFOB	572	668	781	584	694	800	73	48	81	0.17	0.37	0.083
PFMC	571	659	845	581	688	b	27	27	c	0.044	0.24	b
PFD	572	658	848	582	690	b	30	27	c	0.024	0.37	b
HFE-7300	570	659	772	584	685	787	c	32	c	0.095	0.33	0.035
HFE-7700	565	658	772	576	690	787	c	30	c	0.049	0.55	0.11

a Not soluble b No emission c Not obtained

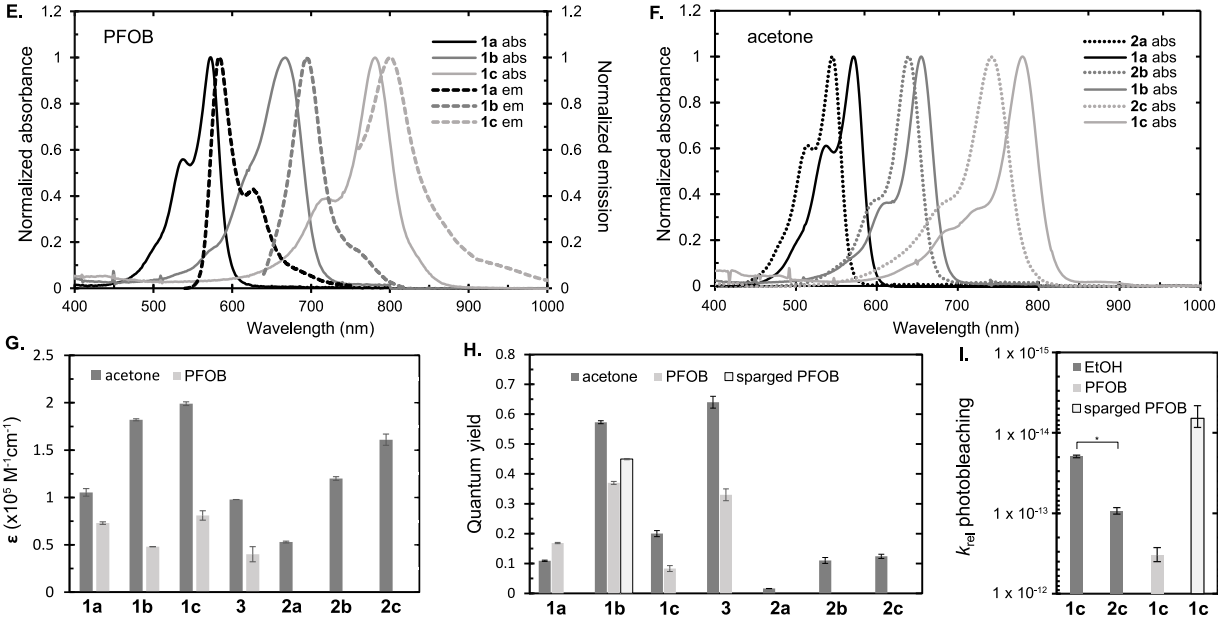

Figure 3. Characterization of cyanine fluorofluorophores **1a**–**1c**. (A) Structure of fluorous rhodamine **3**, used as a benchmark in this study. (B) Solubilities of F_{86}Cy dyes in perfluoromethyl cyclohexane (PFMC) and acetone, and the determination of the fluorous partition coefficient ($\log_F$). Log_F is calculated by the ratio of dye dissolved in PFMC versus toluene. See Figure S3 for the solubility of **2a**–**2c** in acetone. (C) Visible and UV illuminated photographs of investigated dyes in PFMC (top) and acetone (bottom). (D) Table of photophysical properties, where $\lambda_{max,abs}$ is the absorbance maximum, $\lambda_{max,em}$ is the emission maximum, ε is the absorption coefficient, and Φ_F is the fluorescence quantum yield. (E) Absorbance (solid) and emission (dashed) spectra of dyes **1a**–**1c** in perfluorooctyl bromide (PFOB). (F) Absorbance spectra of dyes **1a**–**1c** (solid) and **2a**–**2c** (dashed) in acetone. (G) Absorption coefficients of **1a**–**1c**, **2a**–**2c**, and **3** in acetone and **1a**–**1c** and **3** in PFOB. (H) Quantum yields of **1a**–**1c**, **2a**–**2c**, and **3** in acetone, **1a**–**1c** and **3** in PFOB, and **1b** in Ar-sparged PFOB. (I) Relative photobleaching rates of **1c** and **2c** in EtOH, **1c** in PFOB, and **1c** in N_2-sparged PFOB. *p < 0.0001.

turn dictates the 3,3 modification on the resulting indolenine. We obtained ketone **8** containing two C_6F_{13} fluorous tags by treatment of known nitrile **7**[17] with methyl Grignard (Figure 2B). When ketone **8** was combined with phenyl hydrazine in refluxing acetic acid, desired indolenine **9** was isolated. The crystal structure of **9** (Figure 2C) shows the two fluorous tags extended on either side of the heterocycle, which supports our hypothesis that multiple chains will help surround the final cyanine dyes with fluorous character. Indolenine **9** was alkylated with (perfluorooctyl)propyl iodide to yield **10**. The electron-withdrawing nature of the fluorous chains caused **10** to be isolated as a methylene indoline rather than the expected indolinium **4**. Encouragingly, **10** was soluble in perfluorocarbon solvents (Figure S2).

Fluorous heterocycle **10** was refluxed in acetic anhydride with either 2,6-lutidine or 2,6-di-*tert*-butyl-4-methylpyridine and linkers triethylorthoformate, malonaldehyde bis(phenylimine) **6b**, or glutaconaldehydedianil **6c** to form tri-, penta-, and heptamethine dyes, respectively. Note that trimethine cyanine dyes can be produced by reacting heterocycles with **6a**; however, this approach was not successful with indoline **10**. After combining **10** with suitable linkers, we obtained three fluorous cyanine dyes deemed F_{86}Cy3 (**1a**), F_{86}Cy5 (**1b**), and F_{86}Cy7 (**1c**), where the "F" refers to fluorous, "86" refers to the number of fluorine atoms,

https://dx.doi.org/10.1021/jacs.0c07761
J. Am. Chem. Soc. XXXX, XXX, XXX−XXX

"Cy" refers to the cyanine scaffold, and "3", "5", or "7" refers to the number of methine units between heterocycles. With these fluorous dyes in hand, we set out to characterize the effect of the fluorous chains on solubility and photophysical properties.

Fluorous Solubility. First, we established the fluorous solubility of fluorous cyanines **1a**−**1c** alongside rhodamine **3** (Figure 3A). The fluorous community has defined $\log_F$, log of the partition of compounds between perfluoromethyl cyclohexane (PFMC) and toluene, as a metric for fluorous solubility.[2] All of the fluorous cyanine dyes have positive $\log_F$ values, which demonstrate the preference for the fluorous phase, with F_{86}Cy3 (**1a**) and F_{86}Cy7 (**1c**) fluorofluorophores possessing greater $\log_F$ values than rhodamine **3** (Figure 3B). Unexpectedly, F_{86}Cy5 (**1b**) has less preference for the fluorous phase when partitioned with toluene. However, when examining the solubility limits of fluorophores **1a**−**1c** in PFMC, the F_{86}Cy5 does display good solubility (0.21 mM), 8 times higher than that of fluorous rhodamine **3** (Figure 3B). Consequently, the differences in $\log_F$ value for **1b** as compared to **1a**, **1c**, and **3** are likely more related to relative solubilities in toluene rather than PFMC. Overall, all of the fluorous cyanine dyes display greater solubility in perfluoromethyl cyclohexane than does fluorous rhodamine **3**, the current standard for tracking the fluorous phase in biological environments.[24,25]

While solubility in perfluorocarbons was our primary interest, we also evaluated the solubility of the cyanine fluorofluorophores in a range of solvents (Figures S4−S7). We found that the fluorous cyanine dyes were well-solubilized in acetone and ethanol. Dichloromethane was also a good solvent for F_{86}Cy5 and F_{86}Cy7 dyes. From these studies, we conclude that the three fluorous tags on **1a**−**1c** are sufficient for imparting solubility in perfluorocarbons but did not exclude solubility in organic solvents.

Impact of Fluorous Tags on Photophysical Properties. Before analyzing the new fluorofluorophores in fluorous solvent, we established how the covalently attached fluorous tags impacted the chromophore. Methylene spacers were employed to buffer the electron-withdrawing effects of the fluorous tags on the cyanine chromophore. However, it is known that the effects of fluorous chains can be observed through up to seven methylenes,[28] and other fluorofluorophores with similar methylene spacers have had altered photophysical properties due to the presence of fluorous chains.[18,19] In imaging applications, important photophysical parameters include (1) the $\lambda_{max,abs}$ and $\lambda_{max,ems}$, (2) overall brightness, which is the product of the absorption coefficient (ε) and quantum yield (Φ_F), and (3) the photostability. To assess the effects of perfluorocarbon substitution, the photophysical parameters of hydrocarbon dyes 1,1′,3,3,3′,3′-hexamethyl indocarbocyanine iodide (HICI, **2a**), 1,1′,3,3,3′,3′-hexamethyl indodicarbocyanine iodide (HIDCI, **2b**), and 1,1′,3,3,3′,3′-hexamethyl indotricarbocyanine iodide (HITCI, **2c**) were measured alongside those of cyanines **1a**−**1c** in acetone (Figure 3D−I, Table S1).

Comparing the absorption and emission wavelengths of the fluorinated and nonfluorinated dyes revealed that the addition of the fluorous chains induces a red-shift of ∼20 nm in the absorption of the cyanine dyes (Figure 3D,F). F_{86}Cy5 is the least red-shifted with a 16 nm difference from **2b**, although when examined in wavenumbers the F_{86}Cy5 and F_{86}Cy7 red-shifts are similar at 383 and 372 cm^{-1}, respectively. F_{86}Cy3 displayed the greatest difference in $\lambda_{max,abs}$ with a 26 nm (836 cm^{-1}) bathochromic shift observed, as compared to **2a**. The red-shifts in emission are slightly larger at 28 nm (841 cm^{-1}) and 26 nm (429 cm^{-1}) for **1a** and **1c**, respectively.

Next, we evaluated the differences in the efficiency of absorption as defined by the absorption coefficient (ε) of dyes **1a**−**1c** (Figure 3G). In all fluorous cyanines, we saw an increase in the absorption coefficient calculated at $\lambda_{max,abs}$ as compared to those of the nonfluorinated analogues (**2a**−**2c**). The largest difference was found between F_{86}Cy3 and HICI (1.8-fold) and decreased as the polymethine chain lengthened. Chemical perturbations increasing the absorption coefficient of fluorophores are not well-established in the literature, and the finding that the addition of fluorination will enhance ε may lead to a new approach for fluorophore optimization, irrespective of the need for fluorous solubility. The increased ε upon the addition of fluorine atoms is consistent with a report by Brase and co-workers where cyanine dyes containing two fluorous tags (35−45 wt% F) were prepared.[29]

The other metric that contributes to fluorophore brightness is the fluorescence quantum yield (Φ_F). As was the case for the absorption coefficient, we found that the addition of the fluorous tags increased the quantum yield, with the greatest changes seen in the Cy3 dyes (Figure 3H). F_{86}Cy3 was 6.9-fold more emissive than HICI. F_{86}Cy5 was 5.2-fold more emissive than HIDCI, while F_{86}Cy7 only had 1.6-fold higher Φ_F than HITCI. Increased Φ_F for fluorofluorophores containing fluorous tags has been observed in the literature and was attributed to the decreased vibrational modes accessible for internal conversion when rigid perfluorocarbon chains are appended.[15,16,18,19]

Lastly, we analyzed the effect of the fluorous tags on photostability (Figure 3I). For this property, only F_{86}Cy7 and HITCI were compared, as the heptamethine dyes exhibit the fastest photobleaching rates. These studies were performed by continuous irradiation with a 780 nm LED (85 mW/cm^2) and monitoring the decrease in absorbance. The data were corrected to account for differences in absorptivity of the fluorophores. We found that for the Cy7 scaffold, the addition of the fluorous chains improved the photostability by 4-fold. We believe the increased photostability of the F_{86}Cy7 over HITCI is due to the electron-withdrawing nature of the fluorous tags, which decrease the reactivity of the polymethine chain toward reactive oxygen species.[30] Similar decreased photobleaching has been observed by Armitage and co-workers who have prepared cyanine dyes with perfluorinated indoline heterocycles.[31]

Impact of Fluorous Solvent on Photophysical Properties. The photophysical comparison of the new fluorous cyanine dyes **1a**−**1c** to the organic analogues **2a**−**2c** demonstrates that fluorous tags impart advantageous qualities for imaging, including increased λ_{max}, brightness, and photostability. With an understanding of the role of covalently attached fluorous tags, we proceeded to analyze how fluorous media affects the photophysical properties of **1a**−**1c**. Because of the limited fluorous solubility of many fluorofluorophores, the understanding of the effect of the fluorous phase on photophysical properties is lacking. With cyanines **1a**−**1c** soluble in acetone and fluorous solvents, we gained insight into the impact of fluorous media on photophysical properties.

We analyzed the absorption, emission, ε, and Φ_F of **1a**−**1c** in five different fluorous solvents: perfluoromethyl cyclohexane (PFMC), perfluorooctyl bromide (PFOB), perfluorodecalin (PFD), and HFE-7300 and HFE-7700 (Novec) (see Figure S9 for structures). These solvents were selected due to their use as

https://dx.doi.org/10.1021/jacs.0c07761
J. Am. Chem. Soc. XXXX, XXX, XXX−XXX

a standard in the fluorous community (PFMC),[2] their prominence as the inner phase of perfluorocarbon nanoemulsions (PFOB and PFD),[8] and their applications toward *in vivo* force measurements (HFE-7300 and HFE-7700).[25,32] Upon visual inspection, the fluorous-tagged cyanine dyes appeared soluble in all of these solvents. Yet, the absorption spectra revealed that, with the exception of PFOB, F_{86}Cy7 (**1c**) was aggregated in solution (Figure S6). In PFMC and PFD, a red-shifted, narrow peak indicative of a J-aggregate is observed, while the HFE solvents primarily have a blue-shifted aggregate with a small percentage of red-shifted aggregate present.[33,34] F_{86}Cy5 (**1b**) displayed broadened absorbance in all fluorous solvents; however, concentration-dependent spectra show identical peak shapes, which suggest that this change is not due to aggregation (Figure S10). F_{86}Cy3 (**1a**) does not show any significant differences in absorption between acetone and the six fluorous solvents analyzed (Figures S4 and S6). For all F_{86}Cy dyes, there was little variation in $\lambda_{max,abs}$ and $\lambda_{max,em}$ of monomeric fluorophore when moving from acetone to fluorous solvent.

In contrast to λ_{max} where little solvatochromism was apparent, we did observe changes in the brightness between cyanine dyes **1a**−**1c** dissolved in acetone and fluorous solvent. Both the absorption coefficient and the quantum yield values decreased in the fluorous phase (Figure 3G,H). For the perfluorocarbons, PFD and PFMC, the most significant decreases were observed with 70−85% lower ε and 50−70% lower Φ_F versus acetone. Because of the aggregation observed in the absorbance spectra, values were not calculated for F_{86}Cy7 in PFD or PFMC. For all of the F_{86}Cy dyes, the optimal fluorous solvents were PFOB and HFE-7700. These two solvents are the most polarizable of the fluorous solvents analyzed due to the presence of bromine or oxygen, respectively. For PFOB, the decrease in ε was highly fluorophore dependent with only a 30% decrease observed for F_{86}Cy3 when moving from acetone to PFOB; however, 73% and 59% decreases were observed for F_{86}Cy5 and F_{86}Cy7, respectively (Figure 3D). The Φ_F values showed similar variations with an increase observed for F_{86}Cy3 but a 35% decrease for F_{86}Cy5 and 58% decrease for F_{86}Cy7. In HFE-7700, the ε appears to behave similarly to those in the perfluorocarbons, but the Φ_F values are more comparable to the values in acetone.

The observed decrease in brightness was surprising as the general trend for symmetrical cyanine fluorophores is that more polar solvents lead to decreased Φ_F.[11,35,36] Perfluorocarbons are the most nonpolar solvents, and previous studies had shown increased emission in this phase.[18,19] Further research is ongoing to investigate the unexpected decrease in ε and Φ_F. Fortunately, the disfavored effects of the fluorous phase are countered by the advantageous properties of adding fluorous tags to the cyanine dyes, and the overall brightness of F_{86}Cy3 and F_{86}Cy5 in PFOB is superior to that of HICI and HIDCI in acetone. Furthermore, F_{86}Cy5 (**1b**) is brighter in PFOB than fluorous rhodamine **3**, which demonstrates that we have prepared the brightest, most red-shifted, fluorofluorophore to date.

Next, we evaluated the effect of the fluorous phase on photostability. The photobleaching rates of F_{86}Cy3 (**1a**), F_{86}Cy5 (**1b**), F_{86}Cy7 (**1c**), and fluorous rhodamine **3** in PFOB were measured. We observed the anticipated trend that the stability of the cyanine dyes decreases upon lengthening of the polymethine chain (Table S2 and Figure 3I). Additionally, as consistent with previous studies,[11] the rhodamine scaffold was more stable than the cyanine scaffold (Table S2). Photoirradiation of **1a** and **3** was performed with a 530 nm LED, while **1b** was treated with a 660 nm LED and **1c** was irradiated with a 780 nm LED. The loss of absorbance was monitored over time, and the data were corrected for absorbance differences (see the Supporting Information for further details). Although the decreased photostability in the fluorous phase is consistent with previous findings from our group,[37] these results counter reports of improved photostability of polycyclic aromatics soluble in fluorous solvents.[14]

One of the hallmarks of the fluorous phase is the increased oxygen content (~5 times greater than organic solvent).[38,39] As reactivity with reactive oxygen species is a major photodegradation mechanism for cyanine dyes, it is logical that photobleaching rates would correlate with oxygen concentration.[11,30] When degassed PFOB was employed for the photobleaching of F_{86}Cy7 (**1c**), a 50-fold increase in photostability was observed (Figure 3I). These rates indicate that oxygen content plays a substantial role in the photobleaching mechanism.[40] It should be noted that increased oxygen content has also been shown to decrease Φ_F values.[41−44] We measured the Φ_F in deoxygenated PFOB and likewise observed an oxygen dependence (Figure 3H).

Taken together, the above photophysical insights indicate that fluorous substitution onto cyanine dyes leads to an overall red-shift in absorbance and emission maxima, increased brightness, and increased photostability. When dissolved in perfluorocarbons, brightness and photostability are compromised; however, the λ_{max} and Φ_F values of **1a**−**1c** in perfluorocarbons are comparable to those of dyes **2a**−**2c**, commonly employed as probes for chemical biology and biophysics. With these photophysical insights in hand, we proceeded to evaluate the fluorous cyanines for microscopy studies in cells, 3D multicellular spheroids, and living zebrafish embryonic tissues.

Fluorescent Perfluorocarbon Nanoemulsions. Perfluorocarbon (PFC) nanoemulsions are droplets of fluorous solvent stabilized by surfactant in water. Their initial biomedical utility was oxygen delivery, which received FDA approval in 1989.[45] More recently, PFC emulsions have found applications in ultrasound and magnetic resonance imaging (MRI),[9,46−48] which allow for biodistribution studies in animals but lack the resolution necessary for analyzing trafficking within the cell. Thus, the ability to fluorescently label PFC nanoemulsions provides a complementary analysis tool.

Previously, we have employed fluorous rhodamine **3** to track the cellular internalization and localization of 200 nm PFC nanoemulsions via confocal microscopy.[19,49] While this has been successful, only having one fluorophore available for imaging the nanoemulsions using common confocal laser lines (i.e., 405, 488, 532, or 635 nm)[50] limits the flexibility of multichannel experiments. Additionally, if the loading of rhodamine **3** into the nanoemulsions is too high, aggregation and leakage of the fluorophore is observed.

We envisioned the cyanine fluorofluorophores would overcome these limitations, providing more options for cellular markers and decreasing the likelihood of background from fluorophore leakage. We prepared PFOB-in-water nanoemulsions stabilized by Pluronic F-68 (**11**) containing 0.6 mM **1a**−**1c** or **3** (Figure 4A; see Table S3 for characterization). We used Pluronic F-68 as the surfactant because it

https://dx.doi.org/10.1021/jacs.0c07761
J. Am. Chem. Soc. XXXX, XXX, XXX−XXX

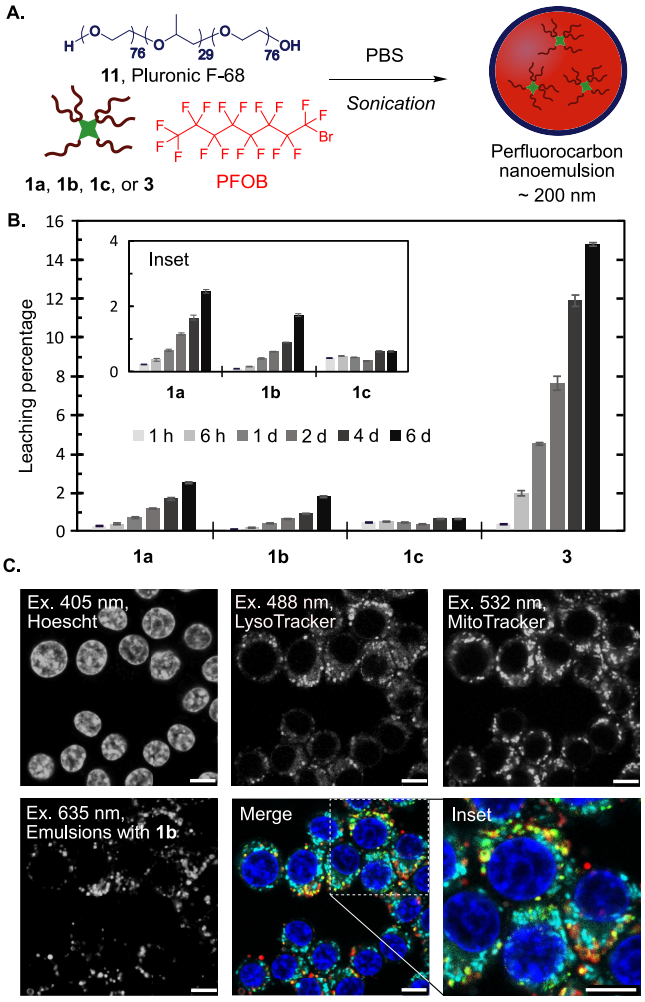

Figure 4. (A) Nanoemulsion preparation entails sonication of PFOB with a fluorofluorophore and Pluronic F-68 in phosphate buffered saline (PBS). (B) The leaching of fluorofluorophores **1a**–**1c** and **3** from PFC nanoemulsions is assayed by rocking an aqueous solution of PFC nanoemulsions containing 0.6 mM fluorofluorophore against 1-octanol. The fluorescence of the 1-octanol layer at 1 h, 6 h, 1 d, 2 d, 4 d, and 6 d is represented as a percentage of total fluorescence in control leaching experiments. (C) Microscopy images of RAW264.7 cells treated with nanoemulsions containing **1b** for 3 h. After treatment, cells were washed and replaced with OptiMEM containing cellular stains. The emulsions containing **1b** (red, ex 635 nm, collect 640–800 nm) are imaged alongside with LysoTracker (green, ex 488 nm, collect 500–530 nm), MitoTracker (cyan, ex 532 nm, collect 540–600 nm), and Hoechst dye (blue, ex 405 nm, collect 420–460 nm). Scale bar = 7.5 μm.

was used in the original FDA-approved formulation[8] and it displays low payload leakage as compared to other commercial and custom surfactants.[51] To analyze the propensity for the fluorofluorophores to leak from the PFOB nanoemulsions, we continuously partitioned aqueous solutions of the nanoemulsions against 1-octanol, a lipid bilayer mimic.[52] The leaching of fluorofluorophores from the PFC nanoemulsions was quantified by measuring the photoluminescence of the 1-octanol layer over time (Figure 4B and Figure S11). All three F_{86}Cy dyes show increased retention within the PFC nanoemulsions, with <3% leaching into 1-octanol over 6 days, in comparison to the ~15% leaching of fluorous rhodamine **3**. These data suggest that the increased fluorous solubility of the cyanine dyes directly correlates to more robust fluorescent labels for PFC nanoemulsions.

The promising loading and retention of the F_{86}Cy dyes in PFC nanoemulsions led us to evaluate the performance of F_{86}Cy5 (**1b**) as a fluorescent label for analyzing the cellular internalization of nanoemulsions. F_{86}Cy5 is a far-red fluorophore and can be excited with a 635 nm laser. A fluorophore's efficiency in an imaging experiment can be predicted by calculating the brightness at the excitation wavelength. For F_{86}Cy5 brightness in PFOB at 635 nm, $(\varepsilon_{635} \times \Phi_F) = 13\,500$ cm^{-1} M^{-1}, is superior to the brightness displayed by rhodamine **3** in PFOB excited at 532 nm, the most relevant microscopy laser line for **3** ($brightness_{532} = 9\,900$ cm^{-1} M^{-1}). While lasers for Cy7 are infrequent on confocal microscopes, the F_{86}Cy5 excited at 635 nm would still be brighter than the F_{86}Cy7 excited at its $\lambda_{max,abs}$. These brightness data suggest that F_{86}Cy5 will provide an optimal signal in confocal microscopy as compared to existing fluorofluorophores.

The far-red properties of F_{86}Cy5 (**1b**) leave the visible region of the electromagnetic spectrum and three common confocal microscopy laser lines available for imaging organelles. In one experiment, we were able to simultaneously image the nanoemulsions and three cellular structures, the nucleus (Hoescht dye, ex 405 nm), lysosomes (LysoTracker, ex 488 nm), and mitochondria (MitoTracker, ex 532 nm) (Figure 4C). As expected, we observed colocalization between the emulsions and lysosomes, which indicated that the nanoemulsions are internalized into cells by endocytosis. Lack of colocalization with the mitochondria and nucleus suggests that the F_{86}Cy5 is retained in the emulsions. We also evaluated the toxicity of the PFC nanoemulsions containing fluorofluorophores **1a**–**1c** by treating RAW264.7 cells for 3 h with emulsions containing the fluorofluorophores, washing, staining with propidium iodide, and analysis by flow cytometry. We did not observe any difference in toxicity for cells containing emulsions with and without fluorofluorophore (Figure S12). Collectively, these data combining the cyanine fluorofluorophores with PFC nanoemulsions suggest F_{86}Cy5 (**1b**) is superior to rhodamine **3** as a result of (1) decreased leaching from the nanoemulsions, (2) superior brightness at relevant excitation wavelengths, and (3) red-shifted absorbance and emission.

Force Measurements in Multicellular Aggregates and Zebrafish Tissues. Another important application of fluorous rhodamine **3** has been facilitating *in vivo* measurements of cellular forces within living tissues. The ability to accurately measure mechanical cues at the cellular scale in a wide range of 3D multicellular systems (e.g., spheroids, organoids, and living tissues) could transform our understanding of many cellular, developmental, and disease processes. We have capitalized on the inert, orthogonal nature of the fluorous phase to engineer a perfluorocarbon (PFC) microdroplet technique to precisely measure endogenous mechanical stresses and spatial variations in tissue material properties *in vivo* and *in situ*.[10,24,25] These techniques allow quantitative mechanobiology studies in the native environment of cells using confocal microscopy.

PFC microdroplets enable absolute measurements of mechanical stresses (both compressive and tensile anisotropic stress) in 3D microenvironments.[10,25,32] When a fluorescently labeled microdroplet is inserted between the cells of a living tissue, adjacent cells exert forces on the droplet, which causes its deformation from the equilibrium spherical shape. Imaging the droplet in 3D using confocal microscopy and performing a

https://dx.doi.org/10.1021/jacs.0c07761
J. Am. Chem. Soc. XXXX, XXX, XXX–XXX

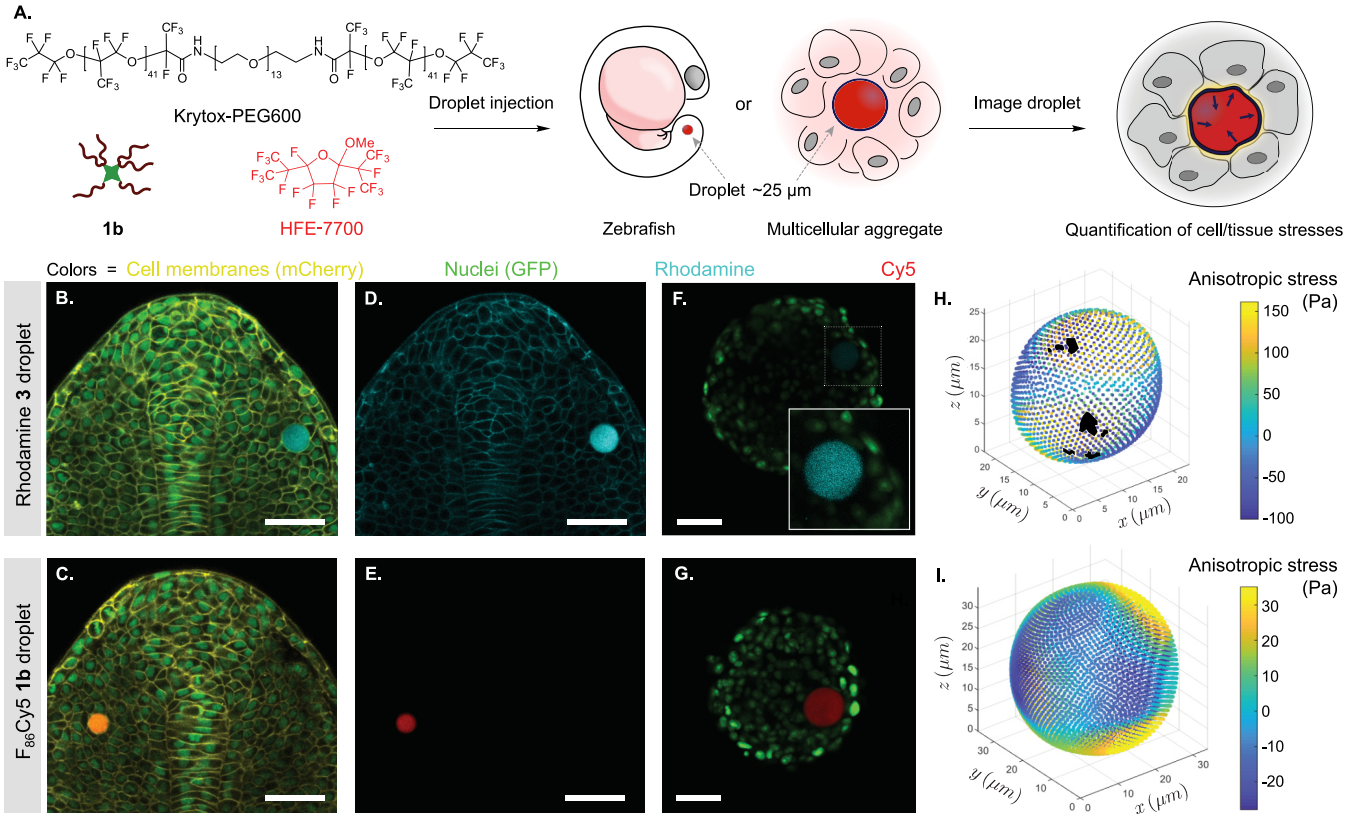

Figure 5. F_{86}Cy5 enhances *in vivo* force measurements in zebrafish embryos and multicellular spheroids. (A) Schematic of the experiment. Surfactant (Krytox-PEG600) and fluorous fluorophore (F_{86}Cy5 **1b** or rhodamine **3**) are diluted in HFE-7700 oil. A single droplet of this mixture is injected either in a zebrafish embryo or in a multicellular spheroid. (B–E) Confocal sections of posterior tissues in developing zebrafish embryos containing a single droplet (10 somite stage). (B,C) Overlay of GFP (nuclei, green), mCherry (membrane, yellow), and rhodamine **3** (droplet, cyan; B) or F_{86}Cy5 **1b** (droplet, red; C). (D,E) Single channel confocal sections of rhodamine **3** (D) and F_{86}Cy5 **1b** (E) labeled droplets from the experiments shown in (B) and (C), respectively. (F,G) Confocal sections through 4T1 multicellular spheroids (nuclei, green) containing droplets labeled with rhodamine **3** (cyan; F) or F_{86}Cy5 **1b** (red; G), imaged with the same power density. The inset in (F) is a magnified region (dashed square) with enhanced droplet signal to make the droplet visible. (H,I) 3D reconstructions of the droplets shown in panels F (H) and G (I), with the magnitude of anisotropic stresses mapped on the droplet surface. (B–G) Scale bars = 50 μm.

high-resolution reconstruction of the droplet shape allows measurements of endogenous mechanical stresses at every point of the droplet surface.[10,32,53] Analysis of droplet deformations (stresses) is performed on 3D fluorescence microscopy images.[53] Therefore, it is key to obtain reliable 3D images of the droplets over time in many different biological environments.

Currently, an important limitation to the force measurements is the quality of fluorescence images, especially for droplets located deep in tissues and/or imaged for long periods. To address these issues, we utilized fluorous cyanine dye **1b** to label droplets in developing zebrafish tissues and in cultured 3D multicellular aggregates (spheroids) and compared our ability to perform accurate force measurements to experiments done with droplets labeled using fluorous rhodamine **3**. A solution of HFE-7700 and Krytox-PEG600, the standard perfluorocarbon and surfactant for *in vivo* force measurements, was prepared. F_{86}Cy5 (**1b**, 0.025 mM) was added, and the mixture was directly microinjected either in zebrafish embryos (10-somite stage) or in previously grown spheroids of 4T1 mouse tumor cells expressing a GFP nuclear marker (Figure 5A; see the Supporting Information for further details). The droplets, as well as different cell structures, were imaged using confocal microscopy (Figure 5B). Cells in contact with droplets containing fluorous cyanines did not show any observable change in behavior and embryos developed normally, as was previously shown for rhodamine **3** labeled droplets.[24,25] Our data show that F_{86}Cy5 (**1b**) is superior to rhodamine **3** in two scenarios: spectral flexibility and photon penetration.

The ability to image the PFC droplets in the far-red region provides orthogonality to standard fluorescent molecular markers commonly employed to generate transgenic lines of different species (zebrafish, mouse, etc.) or cell lines, such as CFP, GFP, YFP, RFP, and mCherry. For precise droplet reconstruction, cross-talk from cellular markers must be minimized. Multiplexed imaging experiments with GFP-labeled nuclei (false colored green), mCherry labeled membranes (false colored yellow), and droplets containing rhodamine **3** (false colored cyan) or F_{86}Cy5 (false colored red) were performed. The merged three color images obtained for droplets in developing zebrafish embryos are shown in Figure 5B (for **3**) and Figure 5C (for **1b**). Single channel confocal sections of the rhodamine **3** droplet channel show substantial signal crosstalk from the mCherry (cell membrane) signal (Figure 5D). In contrast, confocal sections of only the F_{86}Cy5 droplet channel show no crosstalk from other channels (Figure 5E), which indicates that the F_{86}Cy5 dye is clearly superior for droplet reconstruction in these multiplexed imaging experiments.

https://dx.doi.org/10.1021/jacs.0c07761
J. Am. Chem. Soc. XXXX, XXX, XXX−XXX

Finally, we moved to the more challenging system of multicellular spheroids, where the scattering and absorption of light by live tissue hinder imaging, which thereby affects the ability to accurately image the droplets in 3D and perform force measurements. We anticipated that higher quality images would be obtained using F_{86}Cy5 (**1b**) as a result of the lower energy light needed to visualize the droplets and increased brightness of **1b**. Droplets containing either **1b** or **3** were injected into spheroids of mouse 4T1 breast cancer cells expressing a GFP nuclear marker. After droplet insertion, spheroids were cultured for approximately 24 h and then imaged using confocal microscopy. Figure 5F and G shows confocal sections through the spheroids containing the PFC droplet. Exciting both rhodamine **3** (at 543 nm) and F_{86}Cy5 (at 633 nm) with equal power density, we observe a superior signal from the F_{86}Cy5 droplet, consistent with brightness metrics described earlier.

To measure the endogenous cellular forces, the droplet surface was first reconstructed using previously developed algorithms.[53] We then obtained the mechanical anisotropic stresses on the droplet surface (Figure 5H,I) from the measured droplet deformations and the values of interfacial tension measured in each case (see the Supporting Information).[10,53] The better signal of F_{86}Cy5 droplets minimizes surface detection errors and allows for robust force measurements. In contrast, the comparatively low signal of rhodamine **3** droplets leads to surface detection errors, which prevents the measurent of mechanical stresses at some points of the droplet surface (denoted with black patches in Figure 5H). Overall, red-shifted absorbance and advantageous brightness lead to more accurate force measurements in 3D multicellular systems and enable measurements of mechanics deeper in the tissue.

CONCLUSIONS

In this work, we have synthesized cyanine dyes with six perfluoroalkyl substituents, termed F_{86}Cy dyes, to provide the most red-shifted fluorous soluble fluorophores to date. By systematically comparing photophysical traits, we discerned the impact of fluorous substituents and fluorous solvent. The covalent attachment of fluorous tags provides an enhanced absorption coefficient, quantum yield, photostability, and a modest red-shift in absorption and emission. Surprisingly, we found that solubilization in the fluorous phase decreases the brightness of the fluorofluorophores. Despite the unfavorable effects of perfluorocarbon solvents, the F_{86}Cy dyes have photophysical properties comparable to those of cyanine dyes commonly used for microscopy experiments. We employed F_{86}Cy5 (**1b**) for imaging PFC nanoemulsions in cells and PFC microdroplets in 3D multicellular spheroids and developing zebrafish tissues, where the enhanced brightness and far-red emission enable robust measurements of cellular forces in living 3D tissues. The combination of matched excitation wavelengths, the high brightness, and red-shifted absorption of the fluorous cyanine dyes makes them the premier reagents to date for the fluorescent imaging of perfluorocarbons in biological systems.

ASSOCIATED CONTENT

Supporting Information

The Supporting Information is available free of charge at https://pubs.acs.org/doi/10.1021/jacs.0c07761.

Supplemental figures and tables, experimental procedures, and spectral data (PDF)

Crystallographic data for compound **9** (CIF)

AUTHOR INFORMATION

Corresponding Authors

Ellen M. Sletten − *Department of Chemistry and Biochemistry, University of California, Los Angeles, California 90095-1569, United States;* orcid.org/0000-0002-0049-7278; Email: sletten@chem.ucla.edu

Otger Campàs − *Department of Mechanical Engineering, University of California, Santa Barbara, California 93106-5200, United States*; Email: campas@ucsb.edu

Authors

Irene Lim − *Department of Chemistry and Biochemistry, University of California, Los Angeles, California 90095-1569, United States*

Antoine Vian − *Department of Mechanical Engineering, University of California, Santa Barbara, California 93106-5200, United States*

Heidi L. van de Wouw − *Department of Chemistry and Biochemistry, University of California, Los Angeles, California 90095-1569, United States*

Rachael A. Day − *Department of Chemistry and Biochemistry, University of California, Los Angeles, California 90095-1569, United States;* orcid.org/0000-0002-0018-7712

Carlos Gomez − *Department of Mechanical Engineering, University of California, Santa Barbara, California 93106-5200, United States*

Yucen Liu − *Department of Mechanical Engineering, University of California, Santa Barbara, California 93106-5200, United States*

Arnold L. Rheingold − *Department of Chemistry and Biochemistry, University of California, San Diego, California 92093-0505, United States;* orcid.org/0000-0003-4472-8127

Complete contact information is available at: https://pubs.acs.org/10.1021/jacs.0c07761

Notes

The authors declare no competing financial interest.

ACKNOWLEDGMENTS

We thank Monica Pengshung, Margeaux Miller, and Emily Cosco for helpful discussions. We thank Marie Pochitaloff for help in microdroplet injection in zebrafish embryos and Elijah Shelton for help in microdroplet reconstructions. We also thank Sean Megason (Harvard University) for kindly providing the Tg(actb2:memCherry2)^{hm29}, zebrafish transgenic line. This work was supported by NIGMS (5R01GM135380 to E.M.S. and O.C.) and the Sloan Research Foundation (FG-2018-10855 to E.M.S.) A.V. thanks the Swiss National Foundation for financial support (P400PB_191065). We also thank NSF CHE 1048804 for equipment.

REFERENCES

(1) Horváth, I. T.; Rábai, J. Facile Catalyst Separation without Water: Fluorous Biphase Hydroformylation of Olefins. *Science* **1994**, *266*, 72−75.

(2) Horváth, I. T.; Curran, D. P.; Gladysz, J. A. *Handbook of Fluorous Chemistry*; Wiley-VCH: Weinheim, Germany, 2004; pp 1−100.

https://dx.doi.org/10.1021/jacs.0c07761
J. Am. Chem. Soc. XXXX, XXX, XXX−XXX

(3) Gladysz, J. A.; Jurisch, M. Structural, Physical, and Chemical Properties of Fluorous Compounds. In *Fluorous Chemistry*; Horváth, I. T., Ed.; Springer: Berlin, Heidelberg, 2012; pp 1−23.
(4) Yoder, N. C.; Yuksel, D.; Dafik, L.; Kumar, K. Bioorthogonal Noncovalent Chemistry: Fluorous Phases in Chemical Biology. *Curr. Opin. Chem. Biol.* **2006**, *10*, 576−583.
(5) Miller, M. A.; Sletten, E. M. Perfluorocarbons in Chemical Biology. *ChemBioChem* **2020**, DOI: 10.1002/cbic.202000297.
(6) Ko, K.-S.; Jaipuri, F. A.; Pohl, N. L. Fluorous-Based Carbohydrate Microarrays. *J. Am. Chem. Soc.* **2005**, *127*, 13162−13163.
(7) Krishnan, S.; Weinman, C. J.; Ober, C. K. Advances in polymers for anti-biofouling surfaces. *J. Mater. Chem.* **2008**, *18*, 3405−3413.
(8) Castro, C. I.; Briceno, J. C. Perfluorocarbon-Based Oxygen Carriers: Review of Products and Trials. *Artif. Organs* **2010**, *34*, 622−634.
(9) Kaneda, M. M.; Caruthers, S.; Lanza, G. M.; Wickline, S. A. Perfluorocarbon Nanoemulsions for Quantitative Molecular Imaging and Targeted Therapeutics. *Ann. Biomed. Eng.* **2009**, *37*, 1922−1933.
(10) Campàs, O.; Mammoto, T.; Hasso, S.; Sperling, R. A.; O'Connell, D.; Bischof, A. G.; Maas, R.; Weitz, D. A.; Mahadevan, L.; Ingber, D. E. Quantifying Cell-Generated Mechanical Forces within Living Embryonic Tissues. *Nat. Methods* **2014**, *11*, 183−189.
(11) Stennett, E. M. S.; Ciuba, M. A.; Levitus, M. Photophysical Processes in Single Molecule Organic Fluorescent Probes. *Chem. Soc. Rev.* **2014**, *43*, 1057−1075.
(12) Frangioni, J. V. In Vivo Near-Infrared Fluorescence Imaging. *Curr. Opin. Chem. Biol.* **2003**, *7*, 626−634.
(13) In "fluorofluorophores", one "fluoro" refers to fluorine and the other refers to fluorescence. See ref 19.
(14) Sun, H.; Putta, A.; Kloster, J. P.; Tottempudi, U. K. Unexpected Photostability Improvement of Aromatics in Polyfluorinated Solvents. *Chem. Commun.* **2012**, *48*, 12085−12087.
(15) Matsui, M.; Shibata, K.; Muramatsu, H.; Sawada, H.; Nakayama, M. Synthesis, Fluorescence, and Photostabilities of 3-(Perfluoroalkyl)Coumarins. *Chem. Ber.* **1992**, *125*, 467−471.
(16) Matsui, M.; Joglekar, B.; Ishigure, Y.; Shibata, K.; Muramatsu, H.; Murata, Y. Synthesis of 3-Cyano-6-Hydroxy-5-[2-(Perfluoroalkyl)Phenylazo]-2-Pyridones and Their Application for Dye Diffusion Thermal Transfer Printing. *Bull. Chem. Soc. Jpn.* **1993**, *66*, 1790−1794.
(17) Miller, M. A.; Sletten, E. M. A General Approach to Biocompatible Branched Fluorous Tags for Increased Solubility in Perfluorocarbon Solvents. *Org. Lett.* **2018**, *20*, 6850−6854.
(18) Yoshinaga, K.; Swager, T. M. Fluorofluorescent Perylene Bisimides. *Synlett* **2018**, *29*, 2509−2514.
(19) Sletten, E. M.; Swager, T. M. Fluorofluorophores: Fluorescent Fluorous Chemical Tools Spanning the Visible Spectrum. *J. Am. Chem. Soc.* **2014**, *136*, 13574−13577.
(20) Tiers, G. V. D. Perfluoroalkylated Phthalic Anhydride, Copper Phthalocyanine and Their Preparation. U.S. Patent 3281426, October 25, 1966.
(21) Yoshinaga, K.; Delage-Laurin, L.; Swager, T. M. Fluorous Phthalocyanines and Subphthalocyanines. *J. Porphyrins Phthalocyanines* **2020**, *24*, 1074−1082.
(22) Kölmel, D. K.; Hörner, A.; Castañeda, J. A.; Ferencz, J. A. P.; Bihlmeier, A.; Nieger, M.; Brase, S.; Padilha, L. A. Linear and Nonlinear Optical Spectroscopy of Fluoroalkylated BODIPY Dyes. *J. Phys. Chem. C* **2016**, *120*, 4538−4545.
(23) Yang, L.; Adam, C.; Cockroft, S. L. Quantifying Solvophobic Effects in Nonpolar Cohesive Interactions. *J. Am. Chem. Soc.* **2015**, *137*, 10084−10087.
(24) Serwane, F.; Mongera, A.; Rowghanian, P.; Kealhofer, D. A.; Lucio, A. A.; Hockenbery, Z. M.; Campàs, O. In Vivo Quantification of Spatially Varying Mechanical Properties in Developing Tissues. *Nat. Methods* **2017**, *14*, 181−186.
(25) Mongera, A.; Rowghanian, P.; Gustafson, H. J.; Shelton, E.; Kealhofer, D. A.; Carn, E. K.; Serwane, F.; Lucio, A. A.; Giammona, J.; Campàs, O. A Fluid-to-Solid Jamming Transition Underlies Vertebrate Body Axis Elongation. *Nature* **2018**, *561*, 401−405.
(26) Bricks, J. L.; Kachkovskii, A. D.; Slominskii, Y. L.; Gerasov, A. O.; Popov, S. V. Molecular Design of near Infrared Polymethine Dyes: A Review. *Dyes Pigm.* **2015**, *121*, 238−255.
(27) Horvath, I. T. Fluorous Biphase Chemistry. *Acc. Chem. Res.* **1998**, *31*, 641−650.
(28) Jiao, H.; Le Stang, S.; Soos, T.; Meier, R.; Kowski, K.; Rademacher, P.; Jafarpour, L.; Hamard, J.-B.; Nolan, S. P.; Gladysz, J. A. How To Insulate a Reactive Site from a Perfluoroalkyl Group: Photoelectron Spectroscopy, Calorimetric, and Computational Studies of Long-Range Electronic Effects in Fluorous Phosphines $P((CH_2)_m(CF_2)_7CF_3)_3$. *J. Am. Chem. Soc.* **2002**, *124*, 1516−1523.
(29) Braun, A. B.; Wehl, I.; Kolmel, D. K.; Schepers, U.; Brase, S. New Polyfluorinated Cyanine Dyes for Selective NIR Staining of Mitochondria. *Chem. - Eur. J.* **2019**, *25*, 7998−8002.
(30) Gorka, A. P.; Nani, R. R.; Schnermann, M. J. Harnessing Cyanine Reactivity for Optical Imaging and Drug Delivery. *Acc. Chem. Res.* **2018**, *51*, 3226−3235.
(31) Renikuntla, B. R.; Rose, H. C.; Eldo, J.; Waggoner, A. D.; Armitage, B. A. Improved Photostability and Fluorescence Properties through Polyfluorination of a Cyanine Dye. *Org. Lett.* **2004**, *6*, 909−912.
(32) Lucio, A. A.; Mongera, A.; Elijah, Shelton; Chen, R.; Doyle, A. M.; Campàs, O. Spatiotemporal Variation of Endogenous Cell-Generated Stresses within 3D Multicellular Spheroids. *Sci. Rep.* **2017**, *7*, 12022.
(33) Mishra, A.; Behera, R. K.; Behera, P. K.; Mishra, B. K.; Behera, G. B. Cyanines during the 1990s: A Review. *Chem. Rev.* **2000**, *100*, 1973−2001.
(34) Jelly, E. E. Spectral Absorption and Fluorescence of Dyes in the Molecular State. *Nature* **1936**, *138*, 1009−1010.
(35) Berezin, M. Y.; Lee, H.; Akers, W.; Achilefu, S. Near Infrared Dyes as Lifetime Solvatochromic Probes for Micropolarity Measurements of Biological Systems. *Biophys. J.* **2007**, *93*, 2892−2899.
(36) Fluorescence quantum yields are increased in more polar solvents for merocyanines. See: Hoche, J.; Schulz, A.; Dietrich, L. M.; Humeniuk, A.; Stolte, M.; Schmidt, D.; Brixner, T.; Wurthner, F.; Mitric, R. The Origin of the Solvent Dependence of Fluorescence Quantum Yields in Dipolar Merocyanine Dyes. *Chem. Sci.* **2019**, *10*, 11013−11022.
(37) Cao, W.; Sletten, E. M. Fluorescent Cyanine Dye J-Aggregates in the Fluorous Phase. *J. Am. Chem. Soc.* **2018**, *140*, 2727−2730.
(38) Hamza, M. A.; Serratrice, G.; Stebe, M. J.; Delpuech, J. J. Solute-Solvent Interactions in Perfluorocarbon Solutions of Oxygen: An NMR Study. *J. Am. Chem. Soc.* **1981**, *103*, 3733−3738.
(39) Riess, J. G. Understanding the Fundamentals of Perfluorocarbons and Perfluorocarbon Emulsions Relevant to in Vivo Oxygen Delivery. *Artif. Cells Blood Substit. Biotechnol.* **2005**, *33*, 47−63.
(40) Lepaja, S.; Strub, H.; Lougnot, D.-J. Photophysical Study of a Series of Cyanines Part III. The Direct Photooxidation Reaction. *Z. Naturforsch., A: Phys. Sci.* **1983**, *38a*, 56−60.
(41) Lakowicz, J. R. Quenching of Fluorescence. *Principles of Fluorescence Spectroscopy*; Springer-Verlag US: Boston, MA, 2006; pp 277−330.
(42) Potashnik, R.; Goldschmidt, C. R.; Ottolenghi, M. Triplet State Formation in the Quenching of Fluorescence by Molecular Oxygen. *Chem. Phys. Lett.* **1971**, *9*, 424−425.
(43) Olmsted, J. Oxygen Quenching of Fluorescence of Organic Dye Molecules. *Chem. Phys. Lett.* **1974**, *26*, 33−36.
(44) Ware, W. R. Oxygen Quenching of Fluorescence in Solution: An Experimental Study of the Diffusion Process. *J. Phys. Chem.* **1962**, *66*, 455−458.
(45) Krafft, M. P.; Reiss, J. G. Perfluorocarbons: Life Sciences and Biomedical Uses. *J. Polym. Sci., Part A: Polym. Chem.* **2007**, *45*, 1185−1198.
(46) Li, D. S.; Schneewind, S.; Bruce, M.; Khaing, Z.; O'Donnell, M.; Pozzo, L. Spontaneous Nucleation of Stable Perfluorocarbon

https://dx.doi.org/10.1021/jacs.0c07761
J. Am. Chem. Soc. XXXX, XXX, XXX−XXX

Emulsions for Ultrasound Contrast Agents. *Nano Lett.* **2019**, *19*, 173−181.
(47) Akazawa, K.; Sugihara, F.; Nakamura, T.; Matsushita, H.; Mukai, H.; Akimoto, R.; Minoshima, M.; Mizukami, S.; Kikuchi, K. Perfluorocarbon-Based ^{19}F-MRI Nanoprobes for In Vivo Multicolor Imaging. *Angew. Chem., Int. Ed.* **2018**, *57*, 16742−16747.
(48) Koshkina, O.; Lajoinie, G.; Bombelli, F. B.; Swider, E.; Cruz, L. J.; White, P. B.; Schweins, R.; Dolen, Y.; van Dinther, E. A. W.; van Riessen, N. K.; Rogers, S. E.; Fokkink, R.; Voets, I. K.; van Eck, E. R. H.; Heerschap, A.; Versluis, M.; de Korte, C. L.; Figdor, C. G.; de Vries, I. J. M.; Srinivas, M. Multicore Liquid Perfluorocarbon-Loaded Multimodal Nanoparticles for Stable Ultrasound and ^{19}F-MRI Applied to In Vivo Cell Tracking. *Adv. Funct. Mater.* **2019**, *29*, 1806485.
(49) Estabrook, D. A.; Ennis, A. F.; Day, R. A.; Sletten, E. M. Controlling Nanoemulsion Surface Chemistry with Poly(2-Oxazoline) Amphiphiles. *Chem. Sci.* **2019**, *10*, 3994−4003.
(50) Claxton, N. S.; Fellers, T. J.; Davidson, M. W. Laser Scanning Confocal Microscopy. *Encyclopedia of Medical Devices and Instrumentation*; John Wiley & Sons: New York, 2006; pp 449−477.
(51) Day, R. A.; Estabrook, D. A.; Wu, C.; Chapman, J. O.; Togle, A. J.; Sletten, E. M. Systematic Study of Perfluorocarbon Nanoemulsions Stabilized by Polymer Amphiphiles. *ACS Appl. Mater. Interfaces* **2020**, DOI: 10.1021/acsami.0c07206.
(52) Hansch, C.; Fujita, T. ρ-σ-π Analysis. A Method for the Correlation of Biological Activity and Chemical Structure. *J. Am. Chem. Soc.* **1964**, *86*, 1616−1626.
(53) Shelton, E.; Serwane, F.; Campàs, O. Geometrical Characterization of Fluorescently Labelled Surfaces From Noisy 3D Microscopy Data. *J. Microsc.* **2018**, *269*, 259−268.

https://dx.doi.org/10.1021/jacs.0c07761
J. Am. Chem. Soc. XXXX, XXX, XXX−XXX